Advances in Geo-Energy Research

Vol. 19, No. 2, p. 182-196, 2026

Original article

Multi-gate mixture-of-different-experts model for the prediction of multiple properties in multi-phase rocks

Zheng Tang[1], Shuxia Qiu[1]*, Zhili Cai[1], Chung-Lim Law[2], Xin Mao[1], Peng Xu[1,3,4]*

[1]*College of Science, China Jiliang University, Hangzhou 310018, P. R. China*

[2]*Faculty of Innovation and Technology, Taylor's University, Subang Jaya 47500, Malaysia*

[3]*College of Energy Environment and Safety Engineering & College of Carbon Metrology, China Jiliang University, Hangzhou 310018, P. R. China*

[4]*Zhejiang Key Laboratory of Industrial Carbon Metrology Technology Research, Hangzhou 310018, P. R. China*

Keywords:
Multi-phase rock
structural characteristics
permeability prediction
multi-task learning
generative adversarial network

Cited as:
Tang, Z., Qiu, S., Cai, Z., Law, C. -L., Mao, X., Xu, P. Multi-gate mixture-of-different-experts model for the prediction of multiple properties in multi-phase rocks. Advances in Geo-Energy Research, 2026, 19(2): 182-196.
https://doi.org/10.46690/ager.2026.02.06

Abstract:
The prediction of petrophysical properties in multi-phase rock is critical for various geoenergy applications. To this end, deep learning-based methods have recently emerged as a prominent research focus in rock physics. However, due to the inherent scarcity of structural data in multi-phase rocks, coupled with the limitations of convolutional neural network in capturing multi-scale dynamic phase interface and mitigating parameter interference in multi-task learning, predictive performance has not yet reached a satisfactory level. To address this shortcoming, a new multi-task learning framework based on a multi-gate mixture-of-different-experts model is proposed to predict multiple properties of multi-phase rocks. A semi-supervised fractal-informed generative adversarial network is employed to reconstruct multi-phase rocks images, while the finite element method is used to compute their transport properties. The gating network allocates bespoke expert subsets to each task, and an automatic weighted loss function dynamically balances the task-specific loss contributions, enhancing performance and generalization. The results show that the statistical average of the predicted relative permeability aligns with the Brooks-Corey equation, demonstrating the reliability of the proposed model in preserving fundamental physical principles. On the validation dataset, the model achieves high predictive accuracy across all target properties, including fractal dimension, porosity, saturation, permeability of gas phase, permeability of water phase, and effective permeability. Comparative evaluation on the test dataset demonstrates that the proposed model significantly outperforms other multi-task models. These findings confirm that the proposed framework can simultaneously and accurately predict multi-phase rock properties under limited data conditions, holding a promise for guiding assessments in hydrocarbon and geothermal exploration, CO_2 sequestration, nuclear waste disposal, and geological hazard mitigation, among others.

1. Introduction

The petrophysical properties of multi-phase rocks are crucial in hydrocarbon reserve assessment, subsurface resource recovery optimization, and geological hazard prevention (Cai et al., 2024; Rene et al., 2025). In the context of climate change mitigation and sustainable development, the accuracy prediction of petrophysical properties in multi-phase rocks offers substantial practical value, particularly for advancing carbon-neutrality projects, optimizing subsurface resource utilization, and safeguarding ecological security (Al Balushi and Taleghani, 2022; Du et al., 2023; Chen et al., 2025).

*Corresponding author.
E-mail address: p23080854024@cjlu.edu.cn (Z. Tang); qiushuxia@cjlu.edu.cn (S. Qiu); lily.cai@51job.com (Z. Cai); chung-lim.law@nottingham.edu.my (C. -L. Law); p23080854021@cjlu.edu.cn (X. Mao); xupeng@cjlu.edu.cn (P. Xu).

Received December 2, 2025; revised December 29, 2025; accepted January 23, 2026; available online January 26, 2026.

Yandy Scientific Press

However, the inherent complexity of multi-scale pore structures and multi-phase interfaces profoundly influences fluid storage and migration behaviors in multi-phase rocks systems, which brings challenges to understanding the multi-phase fluid dynamics and predicting the multiple petrophysical properties (Liu et al., 2024; Wang et al., 2024; Yang et al., 2025). It has therefore attracted extensive interdisciplinary research across the energy, environmental and geological sciences (Yin et al., 2022; Ng et al., 2024; Ghedira et al., 2025).

The precise characterization of complex pore structures and interfacial dynamics is critical for understanding the fluid flow mechanisms within multi-phase rocks. In recent years, deep learning algorithms were shown to be able to directly learn the nonlinear mapping between rock structural characteristics and transport properties from experimental or simulation data (Zhao et al., 2024); therefore, they have been widely adopted and vigorously developed for rock structure generation and reconstruction, as well as for the prediction of physical properties (Meng et al., 2023; Alzahrani et al., 2024; Zarin et al., 2025). The synergistic integration of deep learning algorithms with computed tomography (CT) imaging techniques effectively addresses critical challenges such as processing large-scale datasets from high-resolution images and enhancing recognition accuracy with limited data from multi-phase rocks (Kato et al., 2015; Yu et al., 2025). Through a data-driven approach, deep learning-based methods circumvent the need to solve the complex partial differential equations and offer higher computational efficiency, strong multi-scale adaptability, and the ability to handle high-dimensional nonlinear relationships (Siddiqa et al., 2024; Cao et al., 2025; Chakraborty et al., 2025).

Convolutional neural networks (CNNs) have been successfully applied for the prediction of transport properties such as permeability and diffusion coefficients (Wu et al., 2019; Kang et al., 2024; Du et al., 2025). However, CNN-based models typically require large datasets and complex network architectures to achieve satisfactory performance. To address these limitations, a Swin Transformer-based transfer learning model has been proposed for permeability prediction in porous media, demonstrating improved prediction accuracy on small-scale datasets (Geng et al., 2024). Nevertheless, constrained by limited measured porous media data, the optimal model has yet to overcome the impact of complex pore structures on accuracy. Unsupervised learning employs an adversarial neural network to reconstruct rock structures, enabling the generation of high-resolution, near-realistic samples during training without relying on complex Markov chains, thereby it shows potential in mitigating the challenge of limited training samples (Zhang et al., 2024). Since unsupervised learning models are fundamentally constrained by their loss function-dependent evaluation metrics, the integration of physics-informed neural networks has emerged as a promising approach for enhancing model training in nonlinear classification scenarios (Argilaga, 2023a; Hashemi et al., 2024; Montero et al., 2025). These studies collectively demonstrate that a semi-supervised generative adversarial network (GAN) that incorporates physics-informed supervision modules not only augments datasets effectively but also improves feature extraction fidelity in neural networks.

While conventional methodologies excel in single-parameter prediction, their extension to multi-parameter scenarios necessitates sequential model retraining for each additional property, resulting in a linear escalation of computational costs with task complexity, while failing to account for critical interparameter correlations and interdependencies (Han et al., 2023). Multi-task learning (MTL) addresses these issues by enabling the simultaneous optimization of interrelated tasks through shared representation learning. This approach, categorized into soft parameter sharing and hard parameter sharing paradigms (Misra et al., 2016; Liu et al., 2019b; Ruder et al., 2019), has been subsequently applied to simultaneously predict rock porosity, permeability, shear modulus, and bulk modulus (Hu and Sun, 2020; Lee et al., 2021; Cao et al., 2022). However, persistent challenges regarding MTL architectures arise from the inherent nonlinear coupling relationships among unsaturated porous media parameters. These interactions induce task gradient conflicts and negative transfer phenomena, and the data distribution discrepancies may lead to competition in the feature space. Such mechanistic complexities undermine convergence stability and constrain the prediction accuracy of multi-parameter estimation. Recent advances in mixture-of-experts (MoE) architectures have mitigated this limitation by introducing multiple expert networks (Shazeer et al., 2017). Meanwhile, single-gated MoE networks are inherently limited in their ability to effectively control expert weight allocation for diverse tasks. Thus, the multi-gate mixture-of-experts (MMoE) architecture, which employs separate gating networks for each task, thus enabling distinct task-specific combinations of expert networks, demonstrates superior capability in capturing specialized information patterns for different learning objectives (Ma et al., 2018; Hou and Cao, 2022). However, this architecture has not been applied to transport property prediction and cannot capture the relationships between digital rock images and measured physical parameters.

Research has shown that most MTL methods are applied to property prediction in saturated porous media involved a single fluid phase or digital rocks, while they have not been extended to property prediction in multi-phase rocks that contain multiple fluids, where phase interfaces, wettability, and saturation coupling introduce significantly greater modeling complexity. In this study, the prediction of petrophysical properties in multi-phase rocks is intended to support realistic reservoir characterization under non-saturated conditions rather than idealized saturated porous media. Because most subsurface reservoirs operate in multi-phase states, their effective properties cannot be reliably inferred from saturated models or single-phase digital rock analyses, which highlights the necessity of conducting research specifically on multi-phase rocks. Typically, MMoE models include multiple expert layers, with each expert layer sharing the same structure and the overall architecture composed of multi-layer perceptron. However, they have inherent shortcomings in both capturing detailed spatial features within image data and maintaining stable gradients as the network deepens. Therefore, this study presents a new multi-gate mixture-of-different-experts (MMoDE) model and proposes to simultaneously

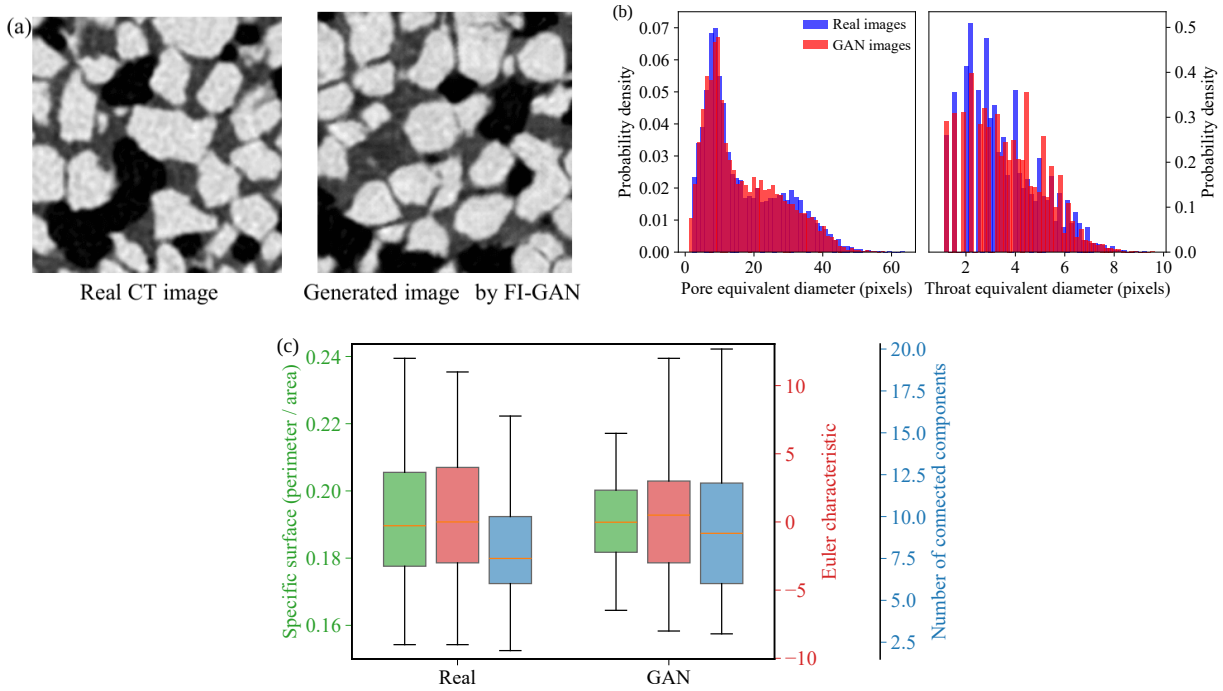

Fig. 1. Comparison between real and generated rock images: (a) Multi-phase rock microstructures, (b) pore and throat size distributions and (c) morphological statistics.

predict multiple physical properties of multi-phase rocks. The fractal informed generative adversarial networks (FI-GAN) is employed to reconstruct multi-phase rocks images, thereby supplementing the dataset (Argilaga, 2023b). Additionally, two different expert network architectures are designed for input feature extraction, and task-specific gating networks are utilized to formulate unique expert combinations for each prediction task. The proposed MMoDE approach not only enables simultaneous multi-parameter prediction but also prevents the accuracy degradation caused by interference when parameters share common features.

2. Data preparation and description

The dataset comprises 10,649 samples, including 2,518 real CT images and 8,131 generated images of multi-phase rocks. The training set includes 7,188 images (2,188 real and 5,000 generated), while the validation set contains 1,349 generated images. To evaluate generalization, the test set consists of 165 unseen real CT images and 891 newly generated images. To ensure strict geological independence, all multi-phase rock images generated by the FI-GAN were derived solely from the training dataset, and real CT images in the test set were neglected during GAN training or data augmentation.

Real images were obtained from X-ray CT scans of quartzite samples with grain diameters of 0.425-0.85 mm (Liu et al., 2019a). Each image was cropped to 184×184 pixels to exclude non-core regions for further processing. The 8,131 synthetic partially saturated quartzite images were generated using a FI-GAN (Argilaga, 2023b) (Fig. 1(a)), whose generator incorporates a fractal dimension-based p-value as a physical constraint alongside the conventional GAN loss, combined via L2-norm into a novel generator loss function. To ensure that the generated images represent realistic geological heterogeneity beyond mere visual similarity, a statistical comparison of key morphological descriptors was conducted between the FI-GAN-generated images and the real CT-scanned samples (Figs. 1(b) and 1(c)). The results indicated a high degree of agreement between the synthetic and real data. As shown in Fig. 1(b), the distributions of pore and throat equivalent diameters from the GAN-generated images closely replicate those of the real samples. Furthermore, other key morphological and topological features (Fig. 1(c)), such as specific surface, Euler characteristic, and the number of connected components, demonstrate strong statistical correspondence between the two datasets. This quantitative validation confirms that the synthetic images successfully capture the critical features of geological realism, ensuring the suitability and reliability of the dataset for training and testing applications.

To segment the gas-water and water-solid interfaces in multi-phase rocks, pixel histograms were drawn to identify the gray-level ranges of each phase. In grayscale images, pixel values are typically represented as 8-bit unsigned integers ranging from [0, 255], where 0 corresponds to black and 255 represents white. The resulting pixel histogram is shown in Fig. 2(a). In the gray-level histogram, different phases often appear as separate peaks or distinct gray-level intervals due to variations in composition, density or imaging modality. The gray-level intervals corresponding to different phases (gas, water, solid) can be determined by examining the peaks and distribution characteristics in the pixel histograms. For segmentation, the gas-water and water-solid threshold were

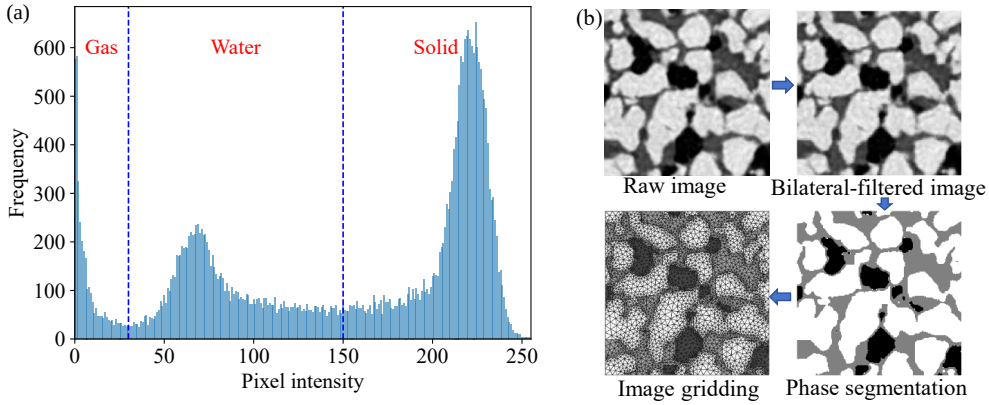

Fig. 2. Phase segmentation: (a) Phase identification of multi-phase rock image based on pixel histogram and (b) image processing workflow.

set at 30 and 150, respectively.

2.1 Structural characteristics

Fractal dimension is a non-integer dimensional value used to quantify the roughness, irregularity or space-filling capacity of complex geometric structures with self-similarity. The box-counting method is one of the most commonly used techniques for this purpose (Liu et al., 2019a), which is expressed as:

$$m(r) \sim r^{-D_f} \tag{1}$$

where m represents the number of boxes needed to cover the fractal object, r represents the size (length) of each box, and D_f is the fractal dimension.

Based on digital image processing techniques, the sample porosity was quantitatively analyzed using a binarization segmentation method. Firstly, the CT raw images were binarized, where the original grayscale image was processed using the Otsu adaptive thresholding algorithm (Otsu, 1975). The I_{bw} of segmented binary images is:

$$I_{bw}(i,j) = \begin{cases} 1 & \text{if } I(i,j) \geq S(\text{matrix region}) \\ 0 & \text{if } I(i,j) < S(\text{pore region}) \end{cases} \tag{2}$$

where S represents the optimal segmentation threshold automatically determined by the Otsu algorithm, and (i,j) denotes the pixel coordinates. The porosity θ is defined as the ratio of the number of pore pixels to the total number of pixels in the image (Russ, 2006):

$$\theta = \frac{N_p}{N_t} = \frac{\sum_{i=1}^{H}\sum_{j=1}^{W}[1 - I_{bw}(i,j)]}{HW} \tag{3}$$

where H and W represent the height and width of the image, respectively, and N_t represents the total number of pixels.

Saturation s_w is a physical quantity that describes the proportion of pore space occupied by a specific fluid phase in a porous medium. It is defined as the ratio of the number of pixels in the water phase region to the total number of pixels in the pore space (Blunt et al., 2013):

$$s_w = \frac{N_w}{N_p} = \frac{N_w}{N_w + N_g} \tag{4}$$

where N represents the number of pixels, and the subscript p, w and g denote pore space, water and gas phases, respectively. Based on the segmentation method described above, the rock image was divided into gas, water and solid phases (Fig. 2(b)).

2.2 Transport properties

Under the assumptions of neglecting inertial effects and gravitational forces in gas-water two-phase flow systems, coupled with incompressible fluid conditions, an elliptical partial differential equation was derived based on the Navier-Stokes equations (Temam, 2024):

$$\mu\left(\frac{\partial^2 u}{\partial X^2} + \frac{\partial^2 u}{\partial Y^2}\right) = \nabla P \tag{5}$$

where X and Y define the Cartesian coordinate system in the image plane. The velocity component u is oriented perpendicularly to this plane, μ represents the dynamic viscosity, and P denotes the pressure. Neglecting hydrodynamic interactions between phases within the flow regime and interfacial dynamics at gas-liquid boundaries in gas-water system simulations, the dynamic viscosity was set to 1 and the pressure gradient was set to 10. A Dirichlet boundary condition $u = 0$ was enforced at the gas-liquid interface due to dominant surface tension effects at the microscale. Within the pore phase, however, this condition was omitted as the homogeneous fluid mixture permits interfacial slip. Neumann boundary conditions were applied along the domain boundaries (Argilaga, 2023b), such as:

$$\frac{\partial u}{\partial n} = q \tag{6}$$

where n denotes the normal vector to the domain boundary, and $\partial u/\partial n$ represents the gradient of the field variable in the normal direction at the boundary. The Neumann parameter $q = 0.05$ was introduced to avoid numerical uncertainties, especially in cases where the fluid domain is entirely enclosed by Neumann boundary conditions.

To solve the partial differential equation using the finite

element method (FEM), different regions in the raw image were firstly segmented into distinct phases. Then, a Gaussian bilateral filter was applied on the image to reduce noise and smooth the features, as illustrated in Fig. 2(b). Using the IM2Mesh tool (Ma, 2019), the filtered image was segmented into solid, water and gas phases. Next, the resulting three-phase raster image was converted into a triangular mesh, with each mesh element retaining its phase label, as illustrated in Fig. 2(b). Sensitivity analyses for both the mesh and boundary conditions were conducted, with the results presented in Table 1. It could be found that the deviation of permeability between the medium mesh and a fine mesh was 0.89%. Therefore, considering the balance between the computational efficiency and accuracy of the results, during mesh generation, the medium mesh was used, and the minimum and maximum edge lengths were set to 2.82 and 50, respectively, with a growth rate of $\sqrt{2}$ and a tolerance of 0.6, while avoiding the activation of sharp corners. The effects of boundary condition variations were investigated with a fixed medium mesh, including changes to the Neumann parameter q (0.01, 0.05, 0.10) and the Dirichlet condition at the gas-liquid interface ($u = 0.1$). The resulting differences in permeability were shown to be minimal, further verifying the stability and robustness of the FEM formulation. By solving Eq. (5) to obtain the velocity u, permeability can be determined according to Darcy's law (Brown, 2002):

$$u = -\frac{K}{\mu}\nabla P \tag{7}$$

where K represents the permeability. The effective permeability K_{eff} can then be calculated as follows (Blunt et al., 2013):

$$K_{eff} = s_w K_w + s_g K_g \tag{8}$$

where s_w and s_g denote the water and gas saturations, and K_w and K_g correspond to the water-phase and gas-phase permeability.

3. MMoDE model

To enable the fast and accurate prediction of multiple petrophysical properties of multi-phase rocks, a new MMoDE model based on MTL with multi-gated MoE is proposed to simultaneously predict the structural characteristics (fractal dimension, porosity and saturation) and transport properties (permeability of gas phase, permeability of water phase and effective permeability).

3.1 MMoDE architecture

The mathematical formulation of MMoE model can be expressed as follows (Ma et al., 2018):

$$y_k = h^k\left[f^k(x)\right] \tag{9}$$

$$f^k(x) = \sum_{i=1}^{e} g^k(x)_i f_i(x) \tag{10}$$

$$g^k(x) = \text{softmax}\left(W_{gk}x\right) \tag{11}$$

where k denotes the k^{th} task; x denotes the input of the model; y_k denotes the output of the k^{th} task; e denotes the total number of expert networks; $f(x)$ represents the shared bottom-network function; h^k is the tower network for task k; $g(x)_i$ indicates the probability (or gating weight) assigned to the i^{th} expert network $f_i(x)$, with $g(x)_i$ constrained to collectively sum to unity; and W_{gk} is the trainable gated matrix. To address the limitations inherent to conventional MMoE frameworks, a new hybrid architecture, MMoDE, was specifically designed for predicting the structural characteristics and transport properties of multi-phase rocks. Specifically, for an expert network containing residual blocks, the output of its unit can be expressed as (He et al., 2016):

Table 1. Mesh and boundary condition sensitivity analysis.

Analysis type	Operating conditions	Permeability (10^{-11} m^2)	Relative change (%)
Mesh type	Coarse	2.756	-2.30
	Medium	2.821	0
	Fine	2.846	0.89
	Very fine	2.853	1.14
Boundary condition	Low q (0.01)	2.821	0
	Default q (0.05)	2.821	0
	High q (0.10)	2.820	-0.04
	No-slip	2.821	0

$$y = F(x) + x \tag{12}$$

where $F(x)$ represents the nonlinear transformation component inside the residual block, x and y represent input and output, respectively. During backpropagation, the gradient propagation formula becomes:

$$\frac{\partial L}{\partial x} = \frac{\partial L}{\partial y}\left[\frac{\partial F(x)}{\partial x} + a\right] \tag{13}$$

where $\partial L/\partial x$ and $\partial L/\partial y$ denote the gradient of the residual block's input x and output y, respectively, and a is the identity matrix corresponding to the identity mapping. Compared to ordinary convolutional layers where $\partial L/\partial x = (\partial L/\partial y)[\partial F(x)/\partial x]$, the residual structure retains a direct gradient component through identity mapping even when gradients are small or approaching zero. This effectively mitigates the vanishing gradient problem and accelerates convergence. Combined with the multi-gate mechanism of MMoE, residual experts and traditional convolutional stacked experts complement each other, jointly enhancing the model's ability to capture multi-scale features in multi-phase rocks images.

The architecture of the proposed MMoDE model is shown in Fig. 3(e). It dynamically combines experts with distinct architectures to extract features at different abstraction levels. The model includes six expert networks, six gating networks, and six tower networks. Experts follow two designs: a residual expert (ExpertRes) with residual blocks, and a deep convolutional expert (ExpertCNN) with stacked convolutional layers. MMoDE is compared with the multi-parameter single-task

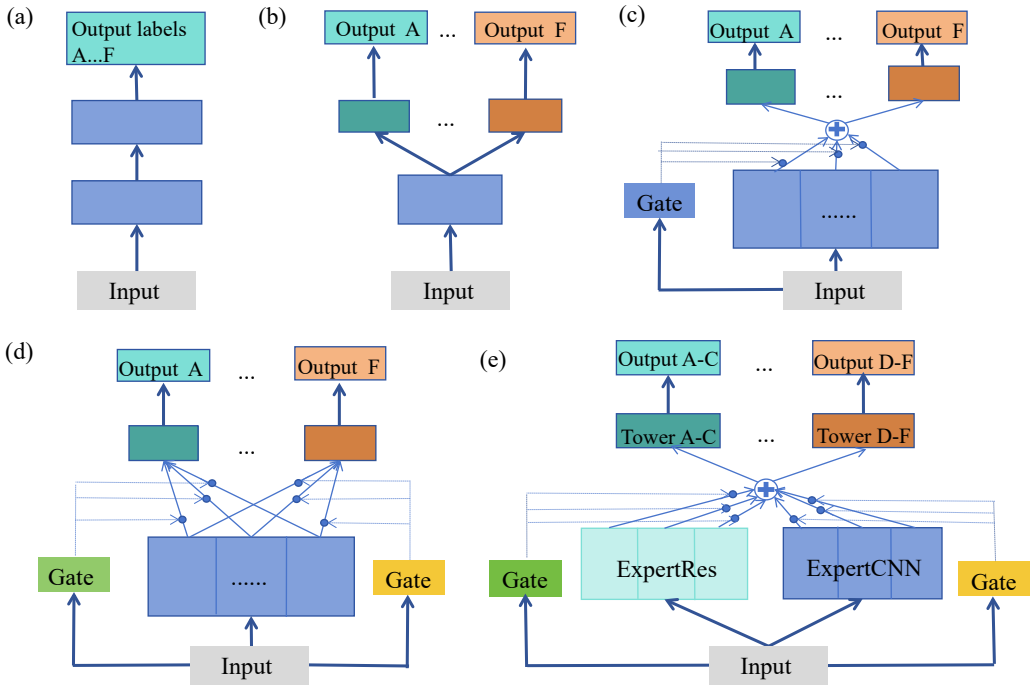

Fig. 3. Schematic graph of MTL networks: (a) MPST, (b) SBM, (c) MoE, (d) MMoE and (e) MMoDE.

model (MPST, Fig. 3(a)), shared-bottom model (SBM, Fig. 3(b)), MoE (Fig. 3(c)), and MMoE (Fig. 3(d)). The single-task model uses one expert and one tower, while MPST shares this structure but outputs multiple parameters. SBM connects a single expert to multiple towers. MoE employs several experts and one gating network, typically with a fusion module for weighted outputs. MMoE extends MoE by using separate gating networks per task, enabling independent expert weighting for each task.

Residual architectures excel at learning hierarchical representations and enhancing feature reuse via identity mappings, whereas convolutional stacks are more effective at capturing local textures and fine-grained details. Accordingly, the proposed MMoDE model incorporates two heterogeneous sets of expert networks to accommodate feature diversity in a multi-task setting. Expert networks built with residual blocks extract features for predicting structural characteristics (fractal dimension, porosity and saturation), while those composed of deep convolutional stacks focus on extracting features for transport properties (multi-phase permeability and effective permeability).

As depicted in the red bounding box of Fig. 4, the residual expert network uses three residual blocks with depthwise separable convolutions. Input passes through a 7×7 convolution and residual blocks with channel dimensions of 64, 128, 256, and 512 sequentially, outputting 2,048-D features via pooling and fully connected layers. The parallel convolutional expert employs multi-scale stacks (kernels 9×9 to 3×3) with ReLU and batch normalization, also producing 2,048-D features for gating compatibility. As illustrated within the gray bounding box of Fig. 4, the gating network dynamically weights expert outputs per task using linear transformations and Softmax, enabling adaptive feature fusion within the multi-expert framework. As depicted by the green bounding box of Fig. 4, each task uses an independent tower network with five hidden layers and ReLU activation, ensuring non-negative outputs for regression. This deep structure supports task-specific decisions while reducing the risks of overfitting from reusing shallow features.

3.2 Loss function and performance indicators

In MTL, the model needs to simultaneously optimize the loss functions of multiple tasks (Ruder et al., 2019):

$$\text{Loss} = \sum_{i=1}^{T} w_i L_i \tag{14}$$

where L_i denotes the loss for the i^{th} task, w_i denotes its corresponding weight, and T is the total number of tasks. The mean squared error (MSE) is used as the loss function for each task:

$$L_i = \frac{1}{t} \sum_{i=1}^{t} (y_i - \hat{y_i})^2 \tag{15}$$

where y_i represents the ground-truth value, $\hat{y_i}$ is the MMoDE prediction, and t denotes the number of samples for each task. The choice of weights has a significant impact on model performance and typically requires manual tuning or hyperparameter optimization, making weight adjustment both inefficient and challenging. Therefore, to account for task-specific uncertainties, a dynamic weight adjustment scheme is used for the overall loss function (Kendall et al., 2018):

$$\text{Loss} = \sum_{i=1}^{T} \left[\frac{1}{2\delta_i^2} L_i + \log\left(1 + \delta_i^2\right) \right] \tag{16}$$

where δ_i represents the uncertainty parameter for the i^{th} task.

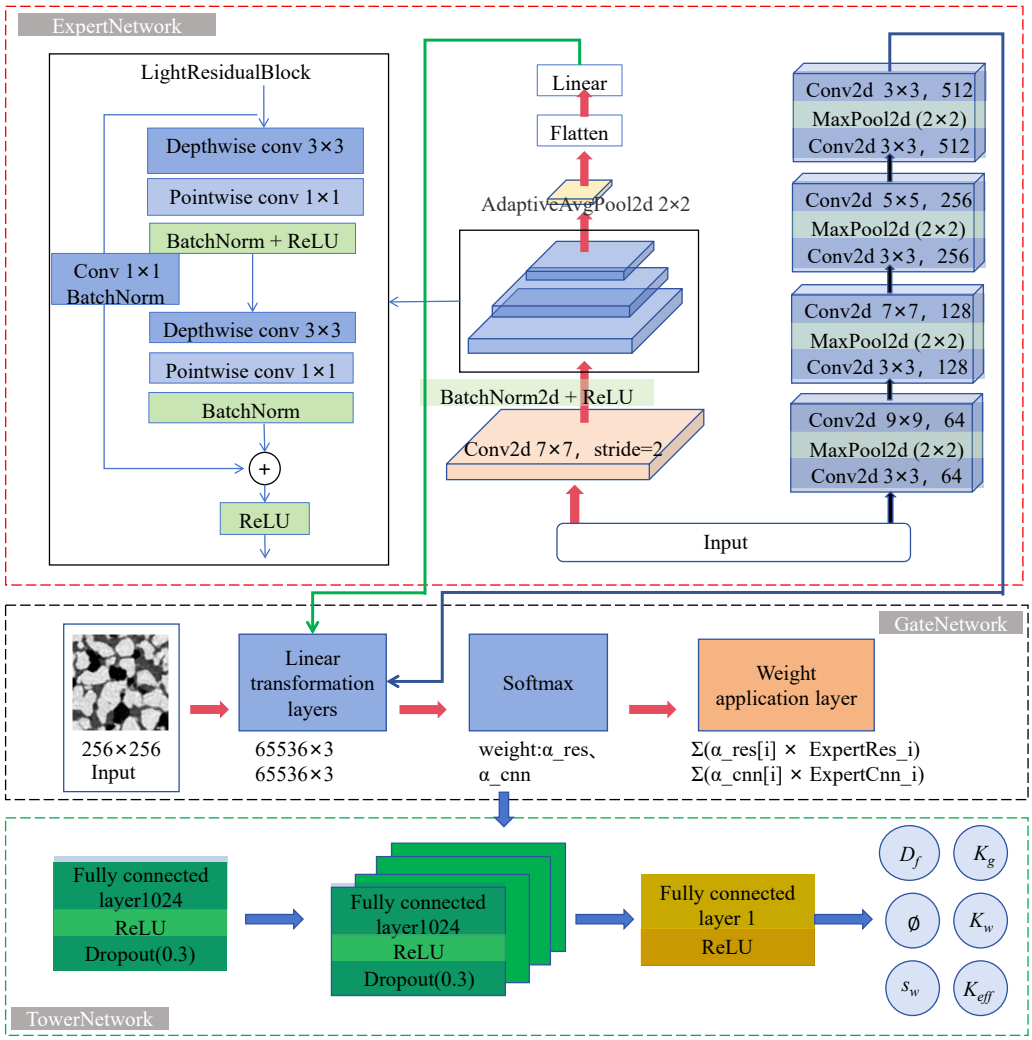

Fig. 4. Architecture of the MMoDE network.

The coefficient of determination was used to measure how well the model fits the data and can be employed to assess its quality (James et al., 2013):

$$R^2 = 1 - \frac{\sum (\hat{y}_i - y_i)^2}{\sum (\overline{y_i} - y_i)^2} \tag{17}$$

where R^2 denotes the coefficient of determination, the numerator is the residual sum of squares, representing the total of squared differences between the true and predicted values, and the denominator is the total sum of squares, representing the total of squared differences between the true values and their mean.

3.3 Model training and testing

This study evaluates one single-task model (MPST) and four deep multi-task models (SBM, MoE, MMoE, and MMoDE). To account for variability in multi-phase rock properties, the input data were normalized using min-max scaling to eliminate dimensional differences and unify data scales. Fig. 5 outlines the MMoDE-based workflow for predicting structural and transport properties. The inputs include raw CT images and FI-GAN-generated images of multi-phase rocks. Using MATLAB for phase segmentation combined with the FEM approach, ground-truth labels were obtained for six tasks: Fractal dimension, porosity, saturation, gas permeability, water permeability, and effective permeability. The dataset was split into 7,188 images for training and 1,349 generated images for validation. Network parameters were updated via backpropagation based on the prediction loss and the chosen optimization algorithm.

All models were implemented in PyTorch (version 2.8.0 with CUDA 12.6 support) and conducted on a 64-bit Windows operating system, running on an AMD Ryzen 7 6800H processor (3.20 GHz). The system was equipped with 32 GB RAM and 1.38 TB NVMe SSD storage. GPU acceleration was provided by an NVIDIA GeForce RTX 3060 Laptop GPU with 6 GB dedicated memory. The model optimization employs the Adam optimizer with a grouped-parameter strategy, together with a dynamic learning rate scheduler. The initial learning rate was set to 0.0001, the training batch size was configured to 32, and the number of training epochs was set to 200. A plateau-aware adaptive learning rate scheduler was used, which reduced the learning rate by a factor of 0.1 whenever

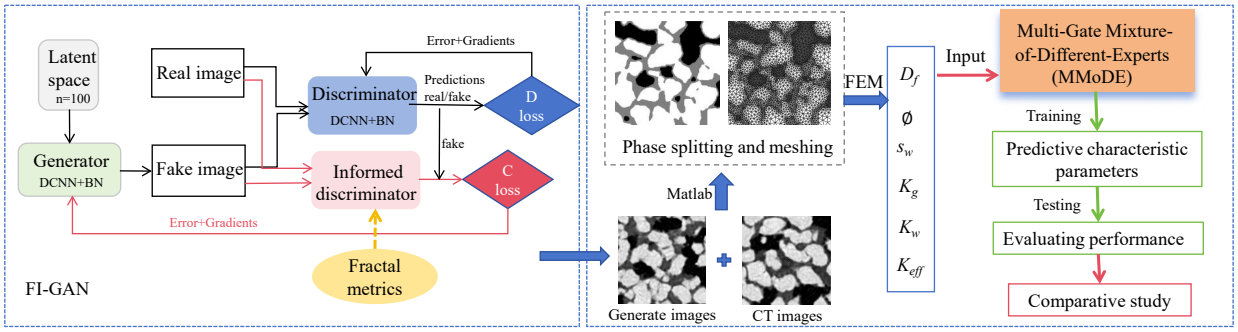

Fig. 5. Workflow of the prediction of structural characteristics and transport properties of multi-phase rocks based on MMoDE.

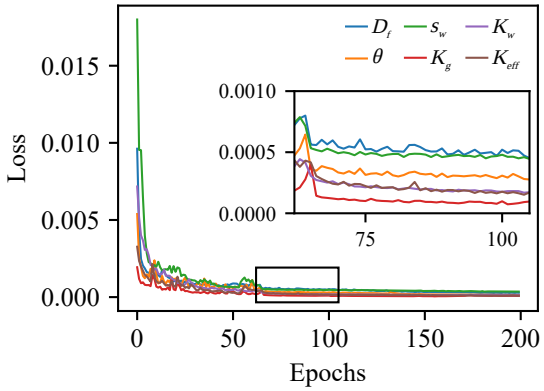

Fig. 6. Training loss of the MMoDE model.

the validation loss failed to improve for 10 consecutive epochs, until reaching a predefined minimum value. This scheme allows the model to use a relatively large learning rate early on to escape local minima, then fine-tune its parameters later with a smaller rate to approach the global optimum. The learning rate is dynamically and automatically adjusted throughout the entire process, with an integrated logging system to track its changes. To visualize the learning process, the training curves of the MMoDE model were plotted in Fig. 6.

4. Results

In this section, the performance of MMoDE in predicting multiple physical properties of multi-phase rocks was evaluated and compared with other MTL approaches and CNN-based single-task models.

4.1 MMoDE performance

The prediction performance of MMoDE on the validation dataset are shown in Fig. 7, the MMoDE model attains R^2 scores of 0.96, 0.98, 0.99, 0.96, 0.89, and 0.89 for fractal dimension, porosity, saturation, permeability of gas phase, permeability of water phase, and effective permeability, respectively. In the prediction of multiple properties, physical properties are not independent but rather exhibit inherent correlations governed by the microstructure of porous media and fluid distribution mechanisms. Therefore, comprehensively evaluating a multi-task prediction model requires not only assessing its accuracy in predicting individual variables but also verifying whether it preserves the essential physical interdependencies among parameters. As shown in Fig. 8, a comparison of the Pearson correlation matrices between the predicted and true values demonstrates that the proposed model effectively maintains several key physical relationships: the strong positive correlation between fractal dimension and porosity reflects the control of pore structural complexity on pore development; the consistent negative correlation between saturation and gas permeability aligns with the phase competition mechanism in multiphase flow; and the high consistency between water permeability and effective permeability indicates that the model accurately captures the contribution of water phase in dominant flow conditions. Furthermore, other weak or negligible correlations are also reliably preserved. The results indicate that the model not only achieves high accuracy in individual parameter prediction but also maintains physically consistent couplings between parameters, demonstrating good physical consistency and systemic reliability. In this way, it meets the requirements for collaborative parameter prediction in practical geological modeling and flow analysis.

To assess whether the proposed model preserves physically meaningful flow behavior in multiphase porous media, a comparative analysis was conducted between the predicted and actual relative permeability curves. As shown in Fig. 9, the predicted and actual relative permeability values are close to each other and follow the same physical trend with saturation. In other words, the water-phase relative permeability increases with saturation, while the gas-phase relative permeability decreases accordingly. It can be observed that the statistical average values of relative permeability are consistent with the Brooks-Corey empirical equation (Xu et al., 2013), with R^2 values around 0.61-0.84 in the fitting results, indicating the reliability of the proposed model in preserving fundamental physical principles.

To evaluate whether the performance gains of MMoDE justify its increased architectural complexity, a single-task CNN baseline (ST-CNN) was constructed as an ablation study. Compared with MMoDE, ST-CNN removes the gating network and bespoke expert subsets, and each target property is predicted by an independently trained CNN sharing the same backbone. As shown in Table 2, ST-CNN consistently underperforms MMoDE across all six target properties, with particularly notable degradation in transport-related parameters. These results indicate that the observed improvements of MMoDE are not merely due to increased model capacity but

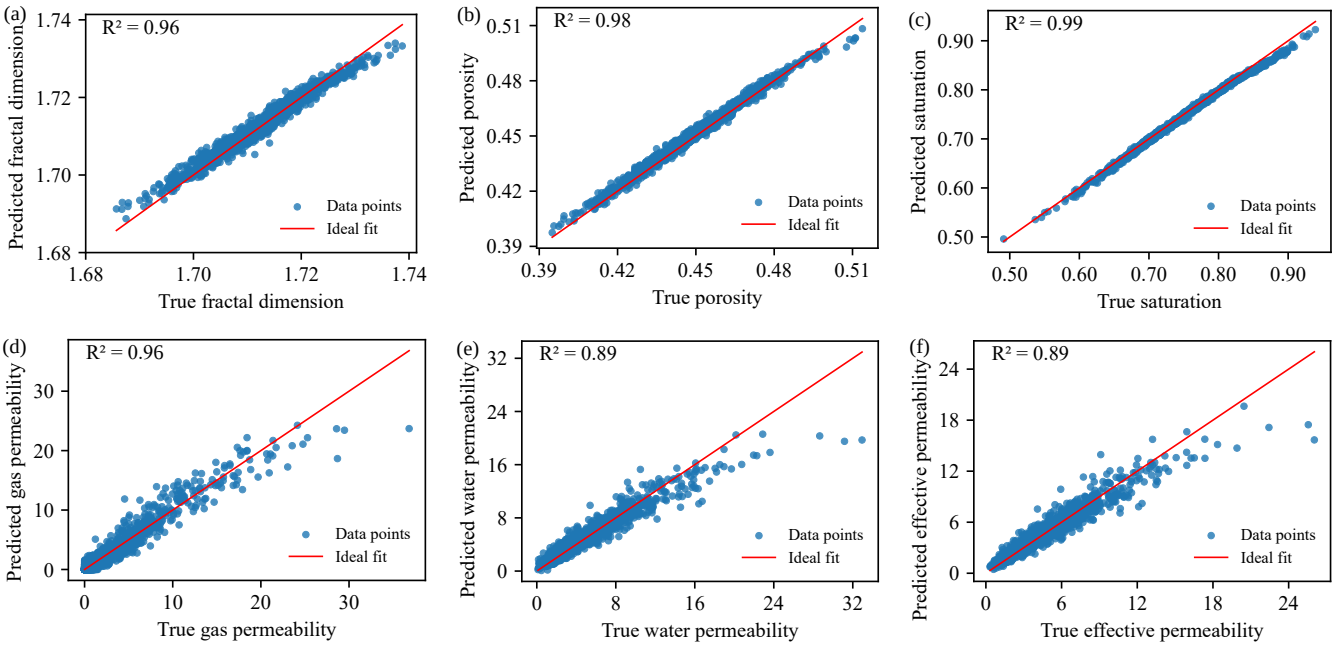

Fig. 7. Prediction performance of MMoDE on the validation dataset: (a) Fractal dimension, (b) porosity, (c) saturation, (d) permeability of gas phase, (e) permeability of water phase and (f) effective permeability.

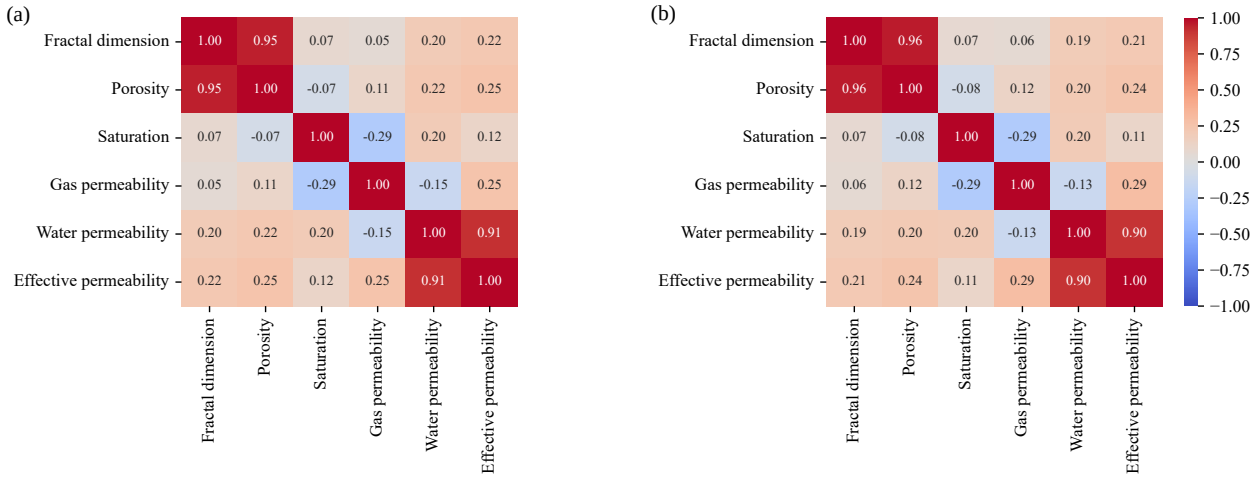

Fig. 8. Pearson correlation heatmap of the true (a) and predicted (b) parameters.

Table 2. Ablation study comparing MMoDE with the single-task CNN baseline.

Model	R^2					
	D_f	θ	s_w	K_g	K_w	K_{eff}
ST-CNN	0.91	0.92	0.97	0.85	0.88	0.69
MMoDE	0.96	0.98	0.99	0.96	0.89	0.89

rather arise from effective task decoupling and adaptive expert selection.

4.2 Performance comparison

Building on the ablation baselines established in the previous section, this section further compares MMoDE with other representative MTL frameworks to provide a more comprehensive architectural analysis. The R^2 scores of the MoE, SBM, MPST, MMoE_CNN, and MMoE_Res models on the validation dataset are summarized in Table 3.

4.2.1 MMoDE versus MoE, SBM and MPST

The prediction performance of MMoDE was firstly compared with that of MoE, SBM and MPST. The single-task CNN model (MPST) with multi-parameter inputs exhibits significantly lower accuracy due to their oversimplified arch-

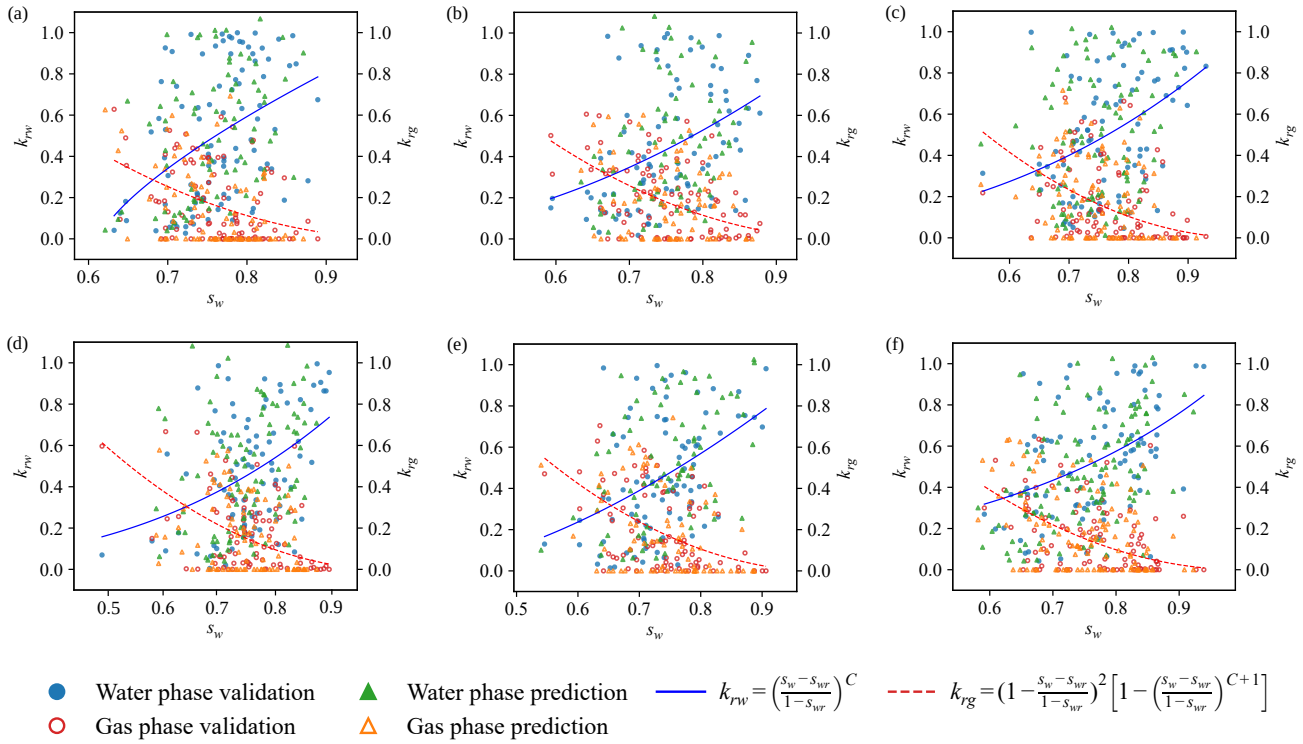

Fig. 9. Comparison between predicted and actual relative permeability at different porosities: (a) $\theta = 0.395$-0.424, (b) $\theta = 0.442$-0.445, (c) $\theta = 0.450$-0.453, (d) $\theta = 0.456$-0.459, (e) $\theta = 0.469$-0.476 and (f) $\theta = 0.476$-0.514.

Table 3. Comparison of performance metrics on the validation dataset.

Model	R^2					
	D_f	θ	s_w	K_g	K_w	K_{eff}
MPST	0.74	0.77	0.89	0.85	0.80	0.79
SBM	0.89	0.93	0.94	0.92	0.89	0.88
MoE	0.90	0.93	0.95	0.92	0.88	0.88
MMoE_Res	0.96	0.98	0.99	0.79	0.83	0.81
MMoE_CNN	0.94	0.94	0.97	0.96	0.91	0.88
MMoDE	0.96	0.98	0.99	0.96	0.89	0.89

itecture. MMoDE achieves R^2 of 0.96 for the prediction of fractal dimension, which is 7%, 8% and 30% higher than that of MoE, SBM and MPST, respectively. In porosity prediction, MMoDE attains R^2 of 0.98 and shows 5%-27% improvement over the other models. For saturation, the R^2 value of MMoDE reaches 0.99, which surpasses the other models by 4%-11%. In permeability-related tasks, MMoDE shows clear advantages, especially in the prediction of gas permeability. The R^2 of MMoDE for gas permeability prediction is 4% higher than that of MoE and SBM, and 13% higher than that of MPST. Through comparative analysis of six-task predictions by MMoDE, MoE, SBM, and MPST, MMoDE consistently outperforms its peers since it effectively leverages latent inter-task correlations in multiple petrophysical parameter prediction. This underscores its enhanced ability to simultaneously capture shared information patterns and task-specific distinctions among petrophysical parameters.

4.2.2 MMoDE versus MMoE

To systematically evaluate the architectural impact of MMoDE on predictive performance, the MMoE model with single-structure expert networks and the proposed MMoDE framework incorporating mixed-of-different-expert networks were compared and analyzed in this section. The MMoE model architecture comprises six expert networks, six gating networks, and six tower networks. The six expert network structures of MMoE_CNN each consists of four convolutional blocks, with each block containing two convolutional layers followed by a max-pooling layer. Meanwhile, the six expert network structures of MMoE_Res are all constructed using residual modules, where each residual block contains two depth-wise separable convolution modules. The other components of MMoE models mirror the MMoDE architecture.

The R^2 of MMoDE for predicting fractal dimension, porosity and saturation on validation dataset is 2%, 4% and 2% higher than that of MMoE_CNN model, respectively. The MMoE_Res model improves the predictive performance for structural characteristics compared to the MMoE_CNN model. However, the MMoE_Res model exhibits a substantial deterioration in the prediction accuracy for transport properties. The predicting accuracy of MMoDE for transport properties (permeability of gas phase, permeability of water phase, and effective permeability) on the validation dataset is 7%-22%

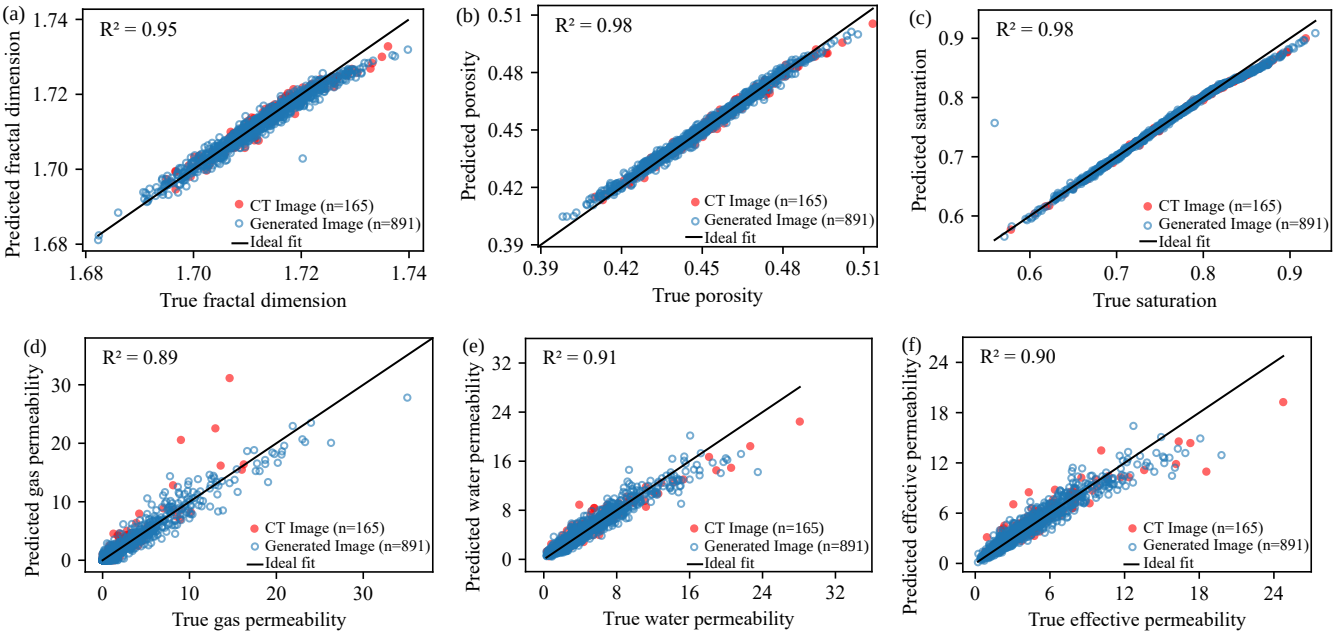

Fig. 10. Predicting performance of MMoDE on the test dataset: (a) Fractal dimension, (b) Porosity, (c) Saturation, (d) Permeability of gas phase, (e) Permeability of water phase and (f) Effective permeability.

higher than that of MMoE_Res model. In summary, compared to MMoE models, the MMoDE model demonstrates superior performance in simultaneously predicting multiple task parameters.

4.3 Generalization capability of MMoDE

To validate the generalization capability of the MMoDE model, the predictive performance of MMoDE, MMoE_CNN, MMoE_Res, MoE and SBM on the test dataset were compared under the same conditions. Fig. 10 shows the performance of MMoDE for six prediction tasks on the test dataset. The MSE, MAE and R^2 score for MMoDE and the other models are summarized in Table 4. Fig. 11 shows the comparison between the relative improvement rates of the MMoDE model and other multitask learning models. Compared with MMoE_CNN, MMoDE reduces the MSE of porosity and fractal dimension tasks by approximately 85% and 21%, respectively, and lowers the MAE by about 64% and 9%. Although the MMoE_Res model achieves comparable performance in predicting structural characteristics with MMoDE, its predictive performance for transport properties is notably poor. The R^2 values of MMoE_Res for gas phase permeability, water phase permeability and effective permeability is 0.69, 0.74 and 0.72, respectively. Furthermore, the MSE and MAE of MMoE_Res are 65%-69% and 43%-54% higher than that of MMoDE, respectively. The R^2 of MMoDE across the six tasks on the test dataset consistently outperforms both MoE and SBM, while its MSE and MAE are substantially lower, indicating superior predictive accuracy and robustness.

The above findings demonstrate that MMoDE significantly outperforms other multi-task models in overall predicting performance on the test dataset. Its dual-structure expert network incorporates diverse feature extraction architectures, with different experts excelling at capturing distinct porous media characteristics. Dynamic gating enhances adaptability to heterogeneous tasks and improves generalization. Notably, the test-set performance of MMoDE for gas permeability declines relative to the validation set. This is because test-set saturations are concentrated between 0.65 and 0.90, meaning that the gas phase occupies a minimal pore volume. Under these high-saturation conditions, gas flow signatures are weak, obscuring the correlation between image features and gas permeability and lowering the R^2. Minor fluctuations and noise in the limited gas phase also increase prediction variance, further reducing R^2.

5. Discussion

The high predictive accuracy of the MMoDE model established across all six task parameters indicates that it offers a significant advantage in modeling multiple petrophysical properties of multi-phase rocks images simultaneously. Compared with MPST, SBM, MoE, and MMoE, the proposed MMoDE indicates the best prediction performance for both structural characteristics and transport properties of multi-phase rocks on both the validation and the test dataset.

In a SBM architecture, all tasks share a single set of feature representations. While this can extract common features to some extent, significant differences between tasks can cause interference during optimization, as the gradient directions for different tasks may conflict, ultimately degrading the overall model performance. On the validation dataset, the highest R^2 value is only 0.94. These results fall below those of other MTL architectures, highlighting the model's limitations in multitask learning scenarios. While the MoE framework partially allevi-

Table 4. Comparison of performance metrics on the test dataset.

Model	Metrics	D_f	θ	s_w	K_g	K_w	K_{eff}
SBM	R^2 score	0.88	0.94	0.94	0.86	0.89	0.88
	MSE	8.38×10^{-6}	1.95×10^{-5}	2.14×10^{-4}	2.57	1.43	1.09
	MAE	2.34×10^{-3}	3.43×10^{-3}	1.16×10^{-2}	0.78	0.79	0.68
MoE	R^2 score	0.92	0.94	0.97	0.87	0.89	0.89
	MSE	5.39×10^{-6}	2.18×10^{-5}	9.32×10^{-5}	2.37	1.43	1.02
	MAE	1.86×10^{-3}	3.70×10^{-3}	7.65×10^{-3}	0.85	0.86	0.71
MMoE_Res	R^2 score	0.94	0.98	0.99	0.69	0.74	0.72
	MSE	3.90×10^{-6}	7.10×10^{-6}	8.7×10^{-6}	5.95	3.65	2.67
	MAE	1.57×10^{-3}	2.11×10^{-3}	2.34×10^{-3}	1.46	1.29	1.12
MMoE_CNN	R^2 score	0.94	0.93	0.97	0.88	0.91	0.90
	MSE	3.84×10^{-6}	2.52×10^{-5}	8.66×10^{-5}	2.24	1.22	0.96
	MAE	1.54×10^{-3}	4.26×10^{-3}	7.51×10^{-3}	0.74	0.71	0.64
MMoDE	R^2 score	0.95	0.98	0.98	0.89	0.91	0.90
	MSE	3.04×10^{-6}	3.89×10^{-6}	6.01×10^{-5}	1.99	1.14	0.93
	MAE	1.40×10^{-3}	1.53×10^{-3}	3.84×10^{-3}	0.67	0.71	0.64

Table 5. Computational cost and resource consumption of different methods.

Cost	STM	MPST	SBM	MoE	MMoE_CNN	MMOE_Res	MMoDE
Parameter size (MB)	280.65	280.65	198.34	573.17	464.65	445.43	653.69
Training time (h)	6	1.02	0.9	4.3	4.4	6.3	5.1
Time cost of single epoch (s)	18.1	18.1	15.9	76.9	79.3	113.4	93.4
Graphic memory consumption (GB)	8	2	2	4	4	4	4
Total time (h)	6	1.02	0.9	4.3	4.4	6.3	5.1

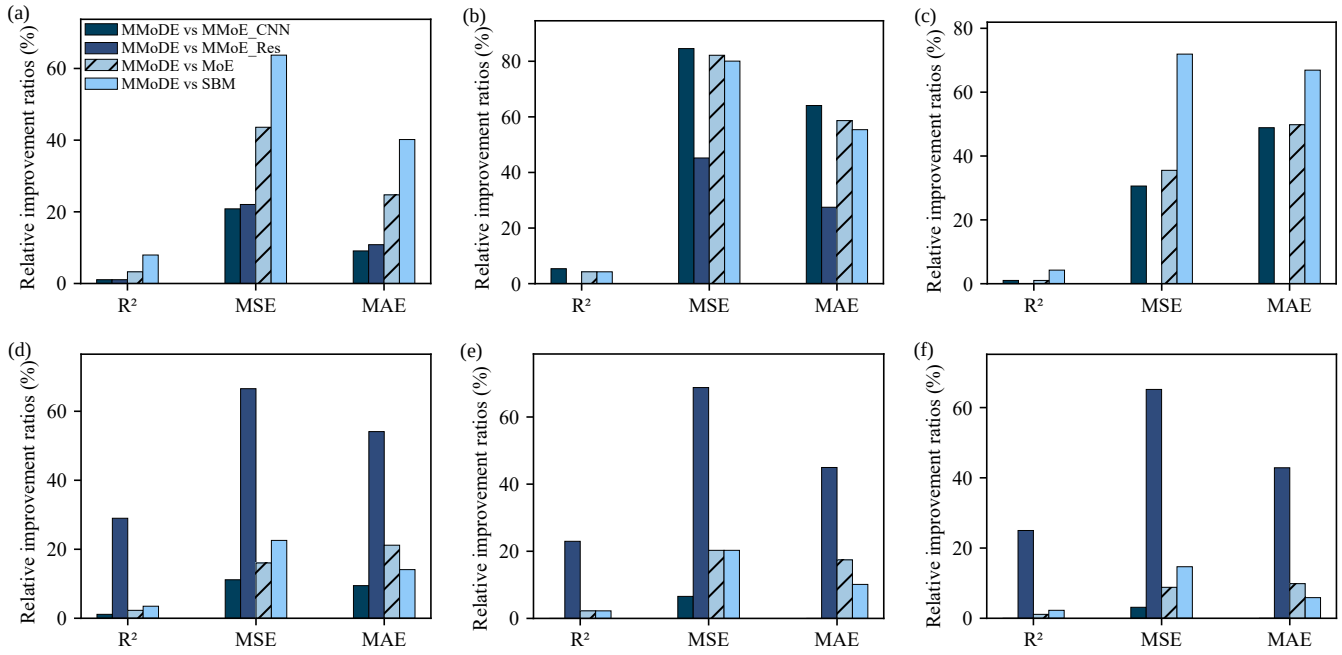

Fig. 11. Relative improvement ratios of different property prediction models for multi-phase rocks: (a) Fractal dimension task, (b) Porosity task, (c) Saturation task, (d) Permeability of gas phase task, (e) Permeability of water phase task and (f) Effective permeability task.

ates task conflicts through multi-expert integration, persistent feature coupling and interference arise when tasks share a unified gating mechanism or exhibit insufficient parameter decoupling among experts. Though exhibiting improvements over SBM, the performance of MoE remains suboptimal compared to the MMoE architecture. The latter addresses these limitations through task-specific gating networks that independently optimize expert weighting for each task. This architectural innovation enhances combinatorial flexibility by enabling selective expert utilization while mitigating inter-task interference through adaptive expert suppression. Overall, the MMoE_CNN model demonstrates improved predictive performance for every task on both the validation and test datasets.

Furthermore, building on the MMoE foundation, MMoDE incorporates residual connections. This hybrid design enables a more effective extraction of complementary structural and flow-related features from the input data, thereby mitigating the bias and overfitting commonly associated with single-architecture models. Residual experts facilitate stable deep-network training by alleviating gradient vanishing and are particularly well-suited for learning global pore structure characteristics, which benefits the prediction of fractal dimension, porosity and saturation. In contrast, convolutional experts progressively capture multi-scale spatial information through enlarged receptive fields, making them more effective for permeability-related predictions and compensating for the limitations of residual structures in modeling flow behavior. As a result, MMoDE achieves the best overall performance on the validation dataset, with R^2 values ranging from 0.89 (K_w and K_{eff}) to 0.99 (s_w), consistently outperforming all baseline models. From a computational perspective, MMoDE requires fewer resources and shorter runtimes than single-task models (STM), as shown in Table 5. Although MMoDE introduces a larger parameter space and incurs higher computational costs than SBM, MoE, MMoE, and MPST due to its decoupled multi-branch expert design, these additional costs are justified by the significant accuracy gains, while it achieves a substantial efficiency advantage over FEM-based methods after full training. It should be noted that the increased model complexity also implies higher data requirements, with effective training requiring at least 5,000 samples, limiting its applicability in extremely small-sample or resource-constrained scenarios. Overall, while simpler architectures are adequate for less complex tasks, MMoDE is better suited for challenging multiphase and multi-modal prediction problems, offering stronger task decoupling, improved generalization, and superior predictive performance.

This study introduces an innovative modeling framework for the efficient prediction of petrophysical properties in multi-phase rock systems. The MMoDE method enables the simultaneous estimation of porosity, saturation, absolute permeability, and relative permeability directly from routine CT images. This provides practical engineering value for applications such as hydrocarbon and geothermal resource assessment, geological CO_2 storage, and geohazard monitoring. While this framework reduces reliance on laboratory tests and improves subsurface simulation fidelity, it also has certain limitations. First, its performance depends on the representativeness of training data, and it entails notable computational and data requirements. Additionally, although the model in its current form focuses on unsaturated rock systems containing water, gas and solid phases, it can be extended to also include oil phases. Future work should focus on extending the model to oil-bearing systems and improving its efficiency for resource-limited scenarios. This may involve techniques such as transfer learning, the integration of physical constraints, or graph neural networks to enhance multi-scale feature learning with less data.

6. Conclusions

In this paper, a novel multi-task MoE model has been developed, aiming to enhance the accuracy and efficiency of predicting multiple petrophysical properties of multi-phase rocks. The proposed MMoDE combines ResNet and CNN as expert networks for different tasks, fully leveraging their complementary advantages. To address the issue of limited datasets, a semi-supervised generator FI-GAN was employed to generate multi-phase rock images, thereby supplementing the real multi-phase rock image data. Comparative experiments were conducted against various MTL models. The main results can be summarized as follows:

1) The MMoDE model significantly outperforms MoE, SBM and MPST in predicting the fractal dimension, porosity, saturation, and permeability of gas phase, and also shows improvement in predicting the permeability of water phase and effective permeability. The predictive performance of MMoDE across all tasks achieves maximum improvements of 7%, 8% and 30% over MoE, SBM and MPST, respectively. The predicted relative permeability averages align with the Brooks-Corey model, confirming the physical consistency of our approach. Besides, MMoDE demonstrates time efficiency advantages over single-task models, that is, training time is reduced by 0.9 hours.
2) The MMoDE model demonstrates superior performance in simultaneously predicting multiple task parameters. Compared to the MMoE_CNN model, it achieves 2%-4% improvement in the prediction of structural characteristics (fractal dimension, porosity, and saturation). Relative to the MMoE_Res model, the MMoDE model exhibits 7%-22% enhancement in the prediction of transport properties (permeability of gas phase, permeability of water phase, and effective permeability).
3) The MMoDE model demonstrates stronger generalization capability compared to other models. Compared with MMoE_CNN and MMoE_Res, MMoDE reduces the MSE by about 3%-85% and 22%-69%, respectively, and it lowers the MAE by 9%-64% and 11%-64%, respectively.

Acknowledgements

This work was jointly supported by the Zhejiang Provincial Natural Science Foundation of China (No. LZ24E060002), the Natural Science Foundation of China (No. 52376079), and the

Fundamental Research Funds for the Provincial Universities of Zhejiang (No. 2024YW109).

Conflicts of interest

The authors declare no competing interest.

References

Al Balushi, F., Taleghani, A. D. Digital rock analysis to estimate stress-sensitive rock permeabilities. Computers and Geotechnics, 2022, 151: 104960.

Alzahrani, M. K., Shapoval, A., Chen, Z., et al. Micro-graphnets: Automated characterization of the micro-scale wettability of porous media using graph neural networks. Capillarity, 2024, 12(3): 57-71.

Argilaga, A. FEM-GAN: A physics-supervised deep learning generative model for elastic porous materials. Materials, 2023a, 16(13): 4740.

Argilaga, A. Fractal informed generative adversarial networks (FI-GAN): Application to the generation of X-ray CT images of a self-similar partially saturated sand. Computers and Geotechnics, 2023b, 158: 105384.

Blunt, M. J., Bijeljic, B., Dong, H., et al. Pore-scale imaging and modelling. Advances in Water Resources, 2013, 51: 197-216.

Brown, G. O. Henry darcy and the making of a law. Water Resources Research, 2002, 38(7): 1106.

Cai, J., Jiao, X., Wang, H., et al. Multiphase fluid-rock interactions and flow behaviors in shale nanopores: A comprehensive review. Earth-Science Reviews, 2024, 257: 104884.

Cao, D., Ji, S., Cui, R., et al. Multi-task learning for digital rock segmentation and characteristic parameters computation. Journal of Petroleum Science and Engineering, 2022, 208: 109202.

Cao, L., Jiang, F., Chen, Z., et al. Data-driven interpretable machine learning for prediction of porosity and permeability of tight sandstone reservoir. Advances in Geo-Energy Research, 2025, 16(1): 21-35.

Chakraborty, A., Rabinovich, A., Moreno, Z. A data-driven physics-informed deep learning approach for estimating sub-core permeability from coreflooding saturation measurements. Advances in Water Resources, 2025, 198: 104919.

Chen, H., Xue, L., Liu, L., et al. Physics-informed graph neural network for predicting fluid flow in porous media. Petroleum Science, 2025, 22(10): 4240-4253.

Du, H., Zhao, Z., Cheng, H., et al. Modeling density-driven flow in porous media by physics-informed neural networks for CO_2 sequestration. Computers and Geotechnics, 2023, 159: 105433.

Du, Q., Zhang, Z., Liu, M., et al. Prediction and optimization of flow and heat transfer performance for helium turbine disc cavity with hybrid deep neural network. International Communications in Heat and Mass Transfer, 2025, 168: 109497.

Geng, S., Zhai, S., Li, C., et al. Swin transformer based transfer learning model for predicting porous media permeability from 2D images. Computers and Geotechnics, 2024, 168: 106177.

Ghedira, A., Lataoui, Z., Benselama, A. M., et al. Numerical simulation of incompressible two-phase flows with phase change process in porous media. Results in Engineering, 2025, 25: 103706.

Han, R., Wang, Z., Guo, Y., et al. Multi-label prediction method for lithology, lithofacies and fluid classes based on data augmentation by cascade forest. Advances in Geo-Energy Research, 2023, 9(1): 25-37.

Hashemi, Z., Gholampour, M., Wu, M. C., et al. A physics-informed neural networks modeling with coupled fluid flow and heat transfer – revisit of natural convection in cavity. International Communications in Heat and Mass Transfer, 2024, 157: 107827.

He, K., Zhang, X., Ren, S., et al. Deep residual learning for image recognition. Paper Presented at the IEEE Conference on Computer Vision and Pattern Recognition, Las Vegas, NV, USA, 27-30 June, 2016.

Hou, Z., Cao, D. Estimating elastic parameters from digital rock images based on multi-task learning with multi-gate mixture-of-experts. Journal of Petroleum Science and Engineering, 2022, 213: 110310.

Hu, C., Sun, B. Multitask learning for petrophysical attributeprediction using convolutional neural network and imbalance dataset. Paper SEG 2020-W13-03 Presented at the SEG International Exposition and Annual Meeting, Virtual, 11-16 October, 2020.

James, G., Witten, D., Hastie, T., et al. An Introduction to Statistical Learning: With Applications in R. Springer Nature, New York, USA, 2013.

Kang, Q., Li, K., Fu, J., et al. Hybrid LBM and machine learning algorithms for permeability prediction of porous media: A comparative study. Computers and Geotechnics, 2024, 168: 106163.

Kato, M., Takahashi, M., Kawasaki, S., et al. Segmentation of multi-phase X-ray computed tomography images. Environmental Geotechnics, 2015, 2(2): 104-117.

Kendall, A., Gal, Y., Cipolla, R. Multi-task learning using uncertainty to weigh losses for scene geometry and semantics. Paper Presented at the IEEE Conference on Computer Vision and Pattern Recognition, Salt Lake City, UT, USA, 18-23 June, 2018.

Lee, J., Kwon, M., Hong, Y. Predicting porosity and water saturation from well-log data using probabilistic multi-task neural network with normalizing flows. Paper OTC 31085 Presented at the Offshore Technology Conference, Virtual and Houston, Texas, 16-19 August, 2021.

Liu, L., Dai, S., Ning, F., et al. Fractal characteristics of unsaturated sands-implications to relative permeability in hydrate-bearing sediments. Journal of Natural Gas Science and Engineering, 2019a, 66: 11-17.

Liu, P., Zhao, J., Li, Z., et al. Numerical simulation of multiphase multi-physics flow in underground reservoirs:

Frontiers and challenges. Capillarity, 2024, 12(3): 72-79.

Liu, S., Johns, E., Davison, A. J. End-to-end multi-task learning with attention. Paper Presented at the IEEE/CVF Conference on Computer Vision and Pattern Recognition, Long Beach, CA, USA, 15-20 June, 2019b.

Ma, J. Im2mesh (2D image to triangular meshes). MATLAB Central File Exchange, 2019.

Ma, J., Zhao, Z., Yi, X., et al. Modeling task relationships in multi-task learning with multi-gate mixture-of-experts. Paper Presented at the 24th ACM SIGKDD International Conference on Knowledge Discovery & Data Mining, London, United Kingdom, 19-23 August, 2018.

Meng, Y., Jiang, J., Wu, J., et al. Transformer-based deep learning models for predicting permeability of porous media. Advances in Water Resources, 2023, 179: 104520.

Misra, I., Shrivastava, A., Gupta, A., et al. Cross-stitch networks for multi-task learning. Paper Presented at the IEEE Conference on Computer Vision and Pattern Recognition, Las Vegas, NV, USA, 27-30 June, 2016.

Montero, F. A. C., Coelho, B. Z., Smyrniou, E., et al. Schemagan: A conditional generative adversarial network for geotechnical subsurface schematisation. Computers and Geotechnics, 2025, 183: 107177.

Ng, C. W. W., Zhou, C., Ni, J. Advanced Unsaturated Soil Mechanics: Theory and Applications. London, UK, CRC Press, 2024.

Otsu, N. A threshold selection method from gray-level histograms. Automatica, 1975, 11: 285-296.

Rene, N. N., Liang, W., Chen, Y., et al. Modeling of multiphase fluids flow in anisotropic rock mass during CO_2 sequestration in fractured reservoirs. Geoenergy Science and Engineering, 2025, 251: 213904.

Ruder, S., Bingel, J., Augenstein, I., et al. Latent multi-task architecture learning. Paper Presented at the Thirty-Third AAAI Conference on Artificial Intelligence, Honolulu, HI, USA, 27-31 January, 2019.

Russ, J. C. The Image Processing Handbook. Boca Raton, USA, CRC Press, 2006.

Shazeer, N., Mirhoseini, A., Maziarz, K., et al. Outrageously large neural networks: The sparsely-gated mixture-of-experts layer. ArXiv Preprint ArXiv: 1701.06538, 2017.

Siddiqa, S., Chang, K., Naqvi, S. B., et al. AI-assisted proton exchange membrane (PEM) fuel cell performance prediction using CFD and data-driven surrogate models. International Communications in Heat and Mass Transfer, 2024, 156: 107616.

Temam, R. Navier-Stokes Equations: Theory and Numerical Analysis. Providence, USA, American Mathematical Society, 2024.

Wang, T., Wang, Y. D., Sun, C., et al. Surface wetting characterization in pore-scale multiphase flow simulations: A ketton carbonate case study. Geoenergy Science and Engineering, 2024, 240: 212933.

Wu, H., Fang, W., Kang, Q., et al. Predicting effective diffusivity of porous media from images by deep learning. Scientific Reports, 2019, 9(1): 20387.

Xu, P., Qiu, S., Yu, B., et al. Prediction of relative permeability in unsaturated porous media with a fractal approach. International Journal of Heat and Mass Transfer, 2013, 64: 829-837.

Yang, M., Wang, D., Dong, Z., et al. Insight into the permeability effect on forced convective heat transfer characteristics in porous media based on the pore-scale numerical study. International Communications in Heat and Mass Transfer, 2025, 165: 109004.

Yin, P., Song, H., Ma, H., et al. The modification of the Kozeny-Carman equation through the lattice Boltzmann simulation and experimental verification. Journal of Hydrology, 2022, 609: 127738.

Yu, Y., Wei, W., Cui, W., et al. Multi-phase segmentation methods for micro-tomographic images based on deep learning. Geoenergy Science and Engineering, 2025, 252: 213962.

Zarin, T., Eshkaftaki, H. A., Sharifi, A. Machine learning-based prediction of oil-water relative permeability using core flooding and CT-scan data. Journal of Molecular Liquids, 2025, 27:105735.

Zhang, T., Bian, N., Liu, Q., et al. 3D super-resolution reconstruction of porous media based on GANs and CBAMs. Stochastic Environmental Research and Risk Assessment, 2024, 38(4): 1475-1504.

Zhao, J., Wu, J., Wang, H., et al. Single phase flow simulation in porous media by physical-informed Unet network based on lattice Boltzmann method. Journal of Hydrology, 2024, 639: 131501.